Thin-Film Photovoltaics Partnership Program

Second Quarterly Status Report – Year III

Covering the period of January 2, 2004 to April 1, 2004

Deliverable: Subcontract Article 3 B, **Item 15 (**ADJ-2-30630-13**)**

Project: **Fundamental Materials Research and Advanced Process Development for Thin-Film CIS-Based Photovoltaics**

P.I.: T. J. Anderson

Co-PI's: Sheng S. Li, O.D. Crisalle, and Valentin Craciun

Other Personnel: Ryan Acher, Ryan M. Kaczynski, Woo Kyoung Kim, Wei Liu, Josh Mangum, Matt Monroe, Zivin Park, Jiyon Song, Xuege Wang, and Seokhyun Yoon

Subcontract No.: ADJ-2-30630-13

Funding Agency: National Renewal Energy Laboratory (NREL)

Program: Thin-Film Photovoltaics Partnership program

Contact Address: Tim Anderson, P.O. Box 116005, 227 Chemical Engineering Bldg., University of Florida, Gainesville FL 32611-6005, Phone: (352) 392-0882, FAX: (352) 392-9513, E-mail: tim@nersp.nerdc.ufl.edu

1 Progress on Reaction Pathways and Kinetics of $CuGaSe_2$ Formation from Bi-layer GaSe/CuSe Precursor Films.

Participants: Timothy J. Anderson and Oscar D. Crisalle (Faculty Advisors), Woo Kyoung Kim, Seokhyun Yoon, Ryan Acher, and Ryan Kaczynski (Graduate Research Assistants).

1.1 Objective

In-situ study of the reaction pathways and kinetics of $CuInSe_2$ formation from bi-layer GaSe/CuSe precursor film using time-resolved, high temperature X-ray diffraction.

1.2 Accomplishments during the current quarter

1.2.1 Preparation of precursor films

Bi-layer GaSe/CuSe precursor films were grown on sodium-free thin (0.4mm) glass substrates in the PMEE (Plasma-assisted Migration Enhanced Epitaxy) reactor. The GaSe bottom layer was grown with a substrate temperature of approximately 250°C. The CuSe top layer was deposited on the as-grown GaSe layer at a lower substrate temperature condition (~150°C) to minimize any potential reactions between the GaSe and CuSe layers. The total thickness (~0.6μm) and the atomic compositions ([Cu]/[Ga] ~1.0 ; [Se]/[Metal] ~1.0) of the bilayer precursor were measured by SEM and ICP respectively.

1.2.2 Time-resolved high temperature X-ray diffraction

Temperature ramp annealing was used to investigate the phase evolution of GaSe/CuSe bilayer precursor. X-ray diffraction data was continuously collected while the sample was heated from 150°C to 350°C in a He ambient. Figure 1-1 demonstrates that GaSe phase is amorphous and the crystalline CuSe phase is transformed to Cu_2Se phase at around 250°C followed by reaction with GaSe to form polycrystalline $CuGaSe_2$ phase. The expected interfacial reaction pathway is

$$2CuSe + 2GaSe \rightarrow Cu_2Se + 2GaSe + Se \rightarrow 2CuGaSe_2 \qquad (1\text{-}1)$$

In the isothermal experiment, the temperature is rapidly ramped to a set point temperature and the isothermal reaction subsequently followed. A set of experiments was performed and a range of set point temperatures was determined such that the experiments were long relative to the scan time but short relative the soaks time (several hours) of the temperature ramp scan. Results are shown in Figure 1-1. To complete the reaction, the temperature was elevated to 500°C and then maintained for about 12 minutes until the reactant CuSe peak disappeared completely and the

product $CuGaSe_2$ peak intensity remained constant. The temperature range for the isothermal experiments was 280°C to 370°C. Kinetic analysis was performed using the Avrami model, which has been widely used to describe solid-to-solid phase transformation. From the Avrami and the Arrhenius plot shown in Figure 1-2, the estimated apparent activation energy of this reaction was around 118 kJ/mol.

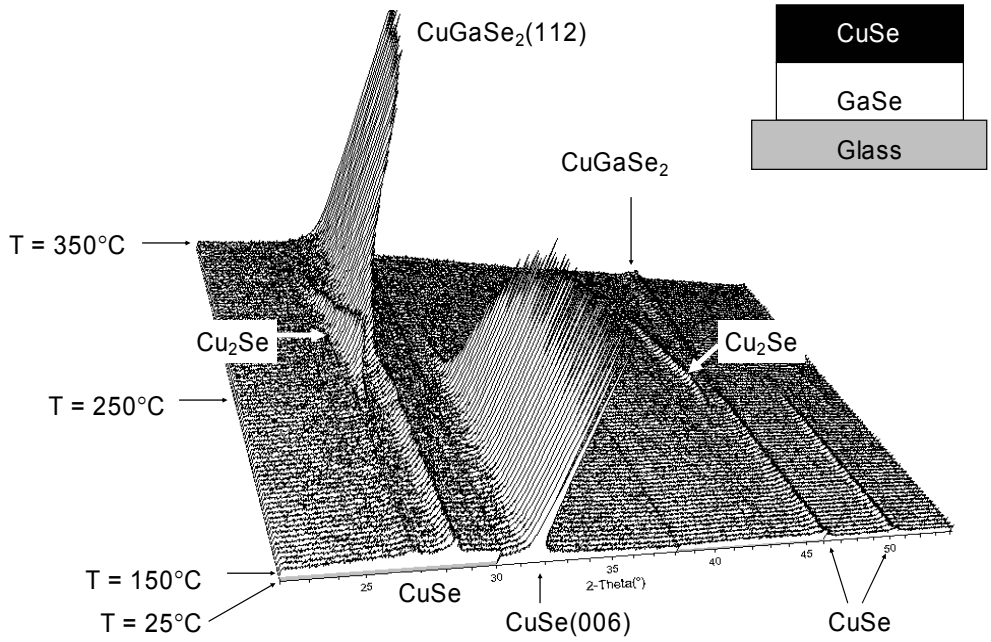

Figure 1-1. X-ray scan during temperature ramp annealing on GaSe/CuSe precursor

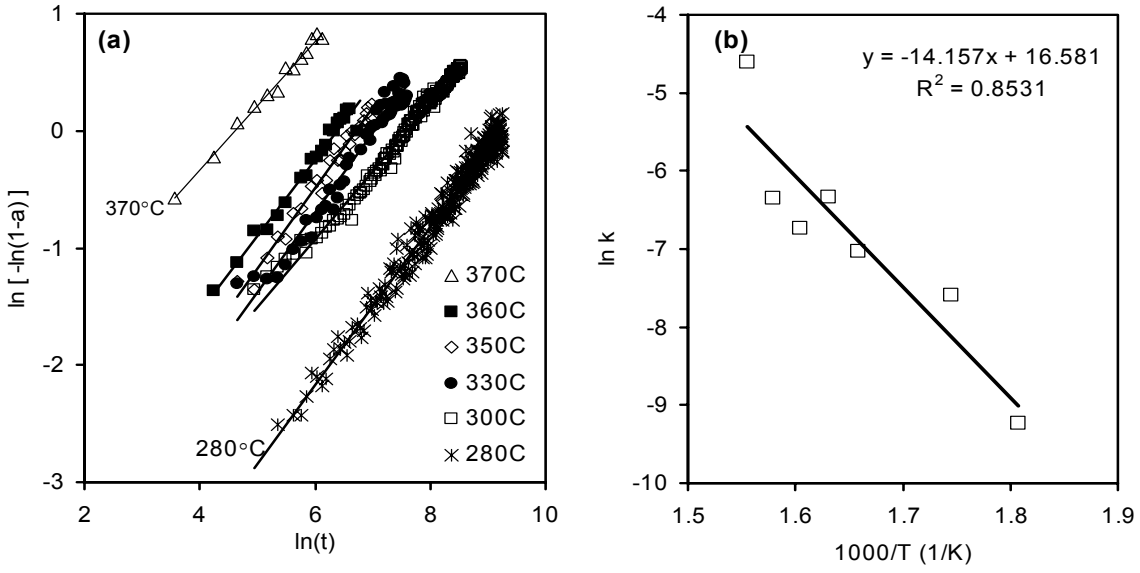

Figure 1-2. (a) Avrami model plot, (b) Arrhenius plot

2 Investigation of Pulsed Non-melt Laser Annealing (NLA) of CIGS-Based Solar Cells

Participants: Sheng S. Li (Faculty Advisor), Xuege Wang, Woo Kyoung Kim, O. D. Crisalle and T. J. Anderson.

2.1 Objectives

To study the effect of Non-melt Laser Annealing (NLA) on the electrical and optical properties of CIS/CIGS based solar cells, and to find the optimal laser annealing condition for improving the cell's performance.

2.2 Accomplishments during the current quarter

The effect of pulsed NLA treatment on the CIGS-based solar cells was investigated under selected annealing conditions. Previous studies showed that several characterization techniques support the conclusion that pulsed NLA treatment under an optimal laser energy density condition can significantly improve the effective carrier lifetime, carrier mobility, surface morphology, spectral response (Q.E.) [1] and hence the cell performance. During this quarter, dark- J-V and DLTS measurements have been carried out to study the effect of NLA treatment on CIGS cells in more detail.

In order to study the effect of pulsed NLA treatment on the diode characteristics between the control cell and NLA treated cells, photo- and dark- J-V measurements were performed at room temperature for all the selected cells. The related theoretical calculations [2,3] of device parameters were carried out for these cells. The measured parameters and calculated values of J_0, n and R_s [4,5] are summarized in Table 2.1 (note R_{sh} is quite high in all tested CIGS cells).

Table 2.1. Device performance parameters determined from the photo-J-V measurements and calculated from the dark- J-V measurements for the control cell and the selected NLA CIGS cells

Cell #	Ctrl-D-C3	CIGS-D1-C3	CIGS-D2-C3
NLA condition	None	30mJ/cm^2, 5 pulses	30mJ/cm^2, 10 pulses
Cell area (cm^2)	0.429	0.429	0.429
V_{oc} (V)	0.528	0.577	0.572
J_{sc} (mA/cm^2)	29.78	34.24	32.00
F.F. (%)	48.86	67.88	66.78
Efficiency (%)	7.69	13.41	12.22
V_m (V)	0.365	0.458	0.453
J_m (mA/cm^2)	21.37	28.99	26.88
N	~4.13	~1.98	~1.96
J_0 (mA/cm^2)	~3.22x10^{-3}	~1.1x10^{-3}	~1.06x10^{-3}
R_s (Ω)	~10.17	~14.06	~15.94

From the dark- J-V curves shown in Figure 2.1, we found that both the dark current density and saturation current density, $J_{0,}$ of the NLA cells are consistently smaller as compared to the control cell. These curves suggest that the recombination current through surface defects dominates the dark- J-V curve under forward bias condition before NLA treatment (with diode ideality factor n >4). After the NLA treatment, a significant reduction in the dark current density was observed due to the reduction of surface defects, and the recombination current was dominated by the bulk defects in the junction space charge region at higher bias (n ≈ 2). This result indicates that defects at the surface region and interface of absorber and buffer layers can be effectively reduced by NLA treatment, thus decrease the recombination of minority carriers via the interface states and defects in the junction space- charge region of the CdS/CIGS cells. Although cells treated by NLA exhibit higher series resistance (R_s), the negative effect of increased R_s on the diode characteristic remains relatively small due to the extremely low value of J_o.

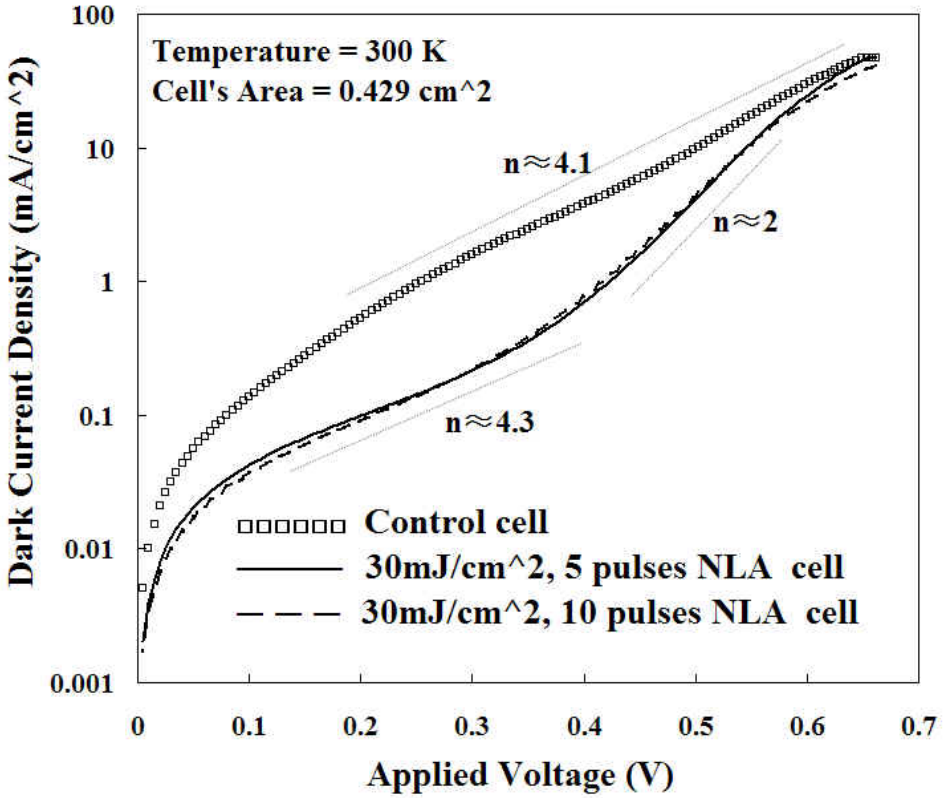

Figure 2.1. The dark- J-V curve (semi-log plot) of the control cell and two NLA treated cells.

In order to investigate the defect property change after NLA processing of CIGS cell, the DLTS and C-V measurements were employed on both the control cell and the NLA cells. The DLTS measurement was performed with a reverse bias (V_R) of 0.5V, a trap-filling pulse amplitude of 0.7V, and a saturation pulse width of 10ms. The DLTS spectra are shown in Figure 2.2 and the DLTS measurement results are summarized in Table 2.2. As shown in Table 2.2, a minority carrier trap with an activation energy of 0.065 ~ 0.069eV, which was quite close to the shallow donor energy level (~0.06eV) known as the selenium vacancy (V_{Se}), was detected and its density was reduced by about 50% after NLA treatment.

Table 2.2 Results of the DLTS measurements on the control and NLA CIGS cells.

	Control cell	**NLA cell (30 mJ/cm^2, 10 pulses)**
Trap type	Minority (electron)	Minority (electron)
Trap activation energy, E_a (eV)	E_c- 0.069	E_c- 0.065
Trap density, N_t (cm^{-3})	5.6×10^{13}	2.8×10^{13}

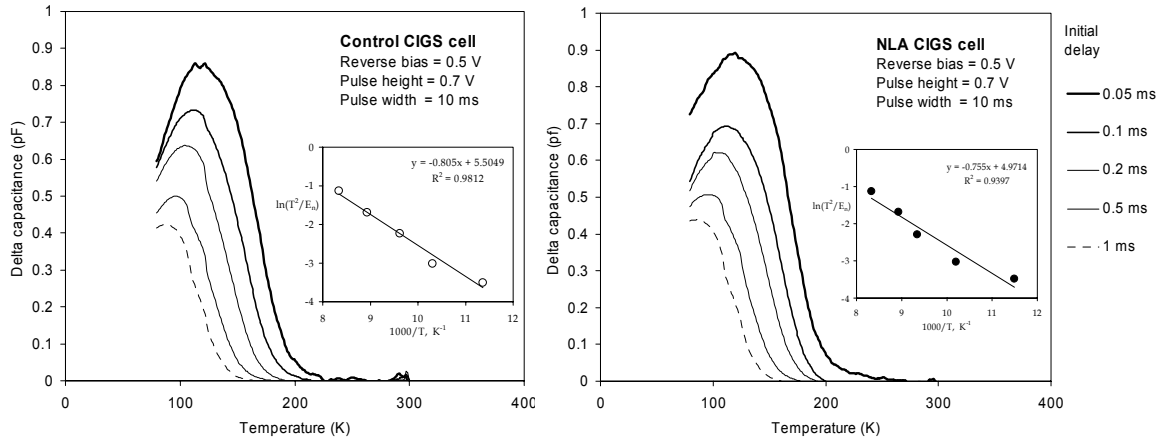

Figure 2.2. The DLTS scans of the control and NLA CIGS cell.

2.3 References

[1] Xuege Wang, Sheng S. Li, C. H. Huang, Lei Li Kerr, S. Rawal, J. M. Howard, V. Cracium, T. J. Anderson, O. D. Crisalle, and R. K. Singh. " Investigation of Pulsed Non-melt Laser Annealing (NLA) of CIGS-Based Solar Cells", *3rd World Conference on Photovoltaic Energy Conversion* (WCPEC-3), Osaka, Japan (2003).

[2] A. Fahrenbruch, R. Bube, Academic Press, New York, 1983.

[3] S.M. Sze, Wiley, New York, 1985.

[4] T. Yanagisawa, T. Kojima, T. Koyanagi, K. Takahisa, D. Nakamura, Elect. Lett. 36 (2000) 1659- 1660

[5] M.K. El-Adawi, I.A. Al-Nuaim, Vacuum 64 (2002) 33-36.

3 Progress on Growth of $Cu(In,Ga)Se_2$ Absorber Films

Participants: Timothy J. Anderson, Oscar D. Crisalle, and Sheng S. Li (Faculty Advisors), and Ryan Kaczynski, Ryan Acher, Woo Kyoung Kim, Seokhyun Yoon (Graduate Research Assistants).

3.1 Objectives

Growth and characterization of $Cu(In,Ga)Se_2$ absorber layers.

3.2 Accomplishments during the current quarter

The PMEE reactor has been prepared for CIGS growth. A literature review of relevant CIGS papers was performed to determine optimal conditions for absorber growth.

3.3 Activities envisioned for the next quarter

An extensive growth plan for CIGS absorber films has been developed to study alternative buffer layers. A maximum of nine substrates can be loaded into the plasma-assisted migration enhanced epitaxy (PMEE) reactor. Mo-coated soda lime glass and bare soda lime glass substrates will be used. The rotation rate of the substrate platen will be set to 12 rpm throughout the entire growth process. Overall compositions of the films will be measured using the inductively coupled plasma (ICP) technique. The copper to gallium+indium mole ratio of the samples will range from Cu-rich to (In,Ga)-rich. Two different processes will be employed to grow CIGS films. The first one will be a constant flux process. The ratio [Cu]/([In]+[Ga]) will remain relatively constant throughout the growth process and the growth temperature will be ~491°C (our maximum substrate temperature). The second process is NREL's 3-layer process. In+Ga+Se will be deposited during the first stage at approximately 400°C, and then Cu and Se will be added at ~491°C until the overall film composition becomes copper-rich. The composition will be returned to Cu-deficient by adding more In+Ga+Se until the desired overall composition is reached. The [Ga]/([In]+[Ga]) ratio will be varied from 0 (CIS) to 1 (CGS) with special attention being paid to absorber films grown with a [Ga]/[In] ratio of approximately 0.3. The absorber thickness will also be varied from 1 μm to 2μm**.**

XRD analysis and cross-sectional SEM will be used to look at the film structure. Electrical measurements such as four probe resistivity and Hall measurements may be carried out on the $CuInGaSe_2$ absorber layers. After deposition of the alternative buffer layer by chemical bath deposition (CBD), the sample will likely be sent to NREL to complete the device fabrication. The finished device will be returned to the University of Florida to determine the Voc, Jsc and cell efficiency.

1 Progress on the Epitaxial Growth of $CuInSe_2$ Absorber Films

Participants: Timothy J. Anderson (Faculty Advisor), and Seokhyun Yoon

3.4 Objectives

Growth of epitaxial $CuInSe_2$ films with different Cu to In ratio and study their defect structure and the electrical properties.

3.5 Accomplishments during the current quarter

The morphology and the crystal structure of the cross section of sample CIS3, previously grown at low substrate temperature of 360 ^{O}C was analyzed by TEM. Bright field image and centered dark field image were shown in Figure 3.1. In Figure 3.1, it is observed that there were very few grain boundaries in matrix region. It is also observed that the boundaries among grains in the island region were extended to the surface of substrate. This means the island regions might be the result of nucleation sites during the early stage of the growth. Selected area diffraction patterns (SADP) for the matrix regions and island regions were taken at zone axis [-1-10], shown in Figure 3.2. There are double spots in SADP for theisland region, which means the grains in island region are slightly mis-oriented or rotated relative to the orientation of the matrix region. However, each grain appeared to be a single crystal.

$CuInSe_2$ films, CIS-A and CIS-B, with different composition were also grown on (100) semi-insulating GaAs substrates. The composition and the growth temperature of each film are shown in Table 3.1. It is observed that both films were grown epitaxially with island structures on the smooth background region, shown by SEM pictures in Figure 3.3. XRD ω-2θ scan also showed there are only (004) and (008) peaks for $CuInSe_2$, which confirms they were grown epitaxially on (100) the GaAs substrate.

3.6 Activities envisioned for the next quarter

The cross-section of CIS-A and CIS-B will be analyzed by TEM to study the morphology and the orientation of the island and matrix regions, respectively. Low temperature photoluminescence study and Hall measurement will also be performed on both samples to see the shallow defects in that film and their relation to the electrical transport properties.

Table 3.1. Composition of $CuInSe_2$ films.

ID	Cu	In	Se	Cu/In	T_{sub}
CIS3	26.68%	24.38%	48.93%	1.09	360 ^{O}C
CIS-A	25.30%	25.58%	49.12%	0.99	465 ^{O}C
CIS-B	26.76%	24.38%	48.87%	1.10	465 ^{O}C

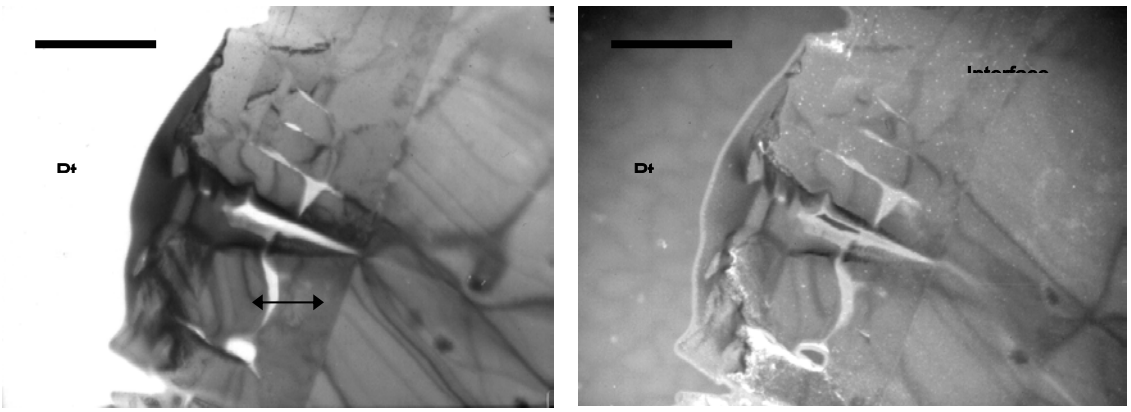

(a) Bright Field image

(b) Centered Dark Field image by diffracted beam from $CuInSe_2$

Figure 3.1. TEM cross-section images of CIS3 after etching.

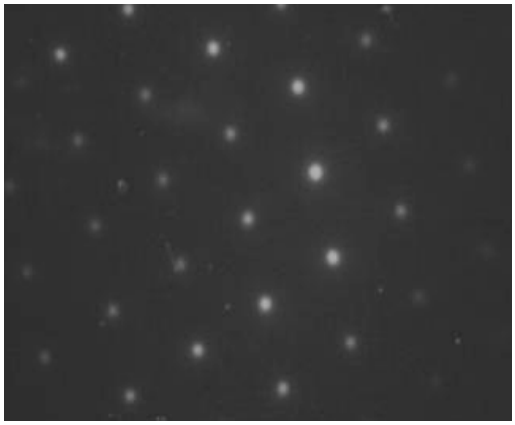

(a) Matrix region : B = [-1-10]

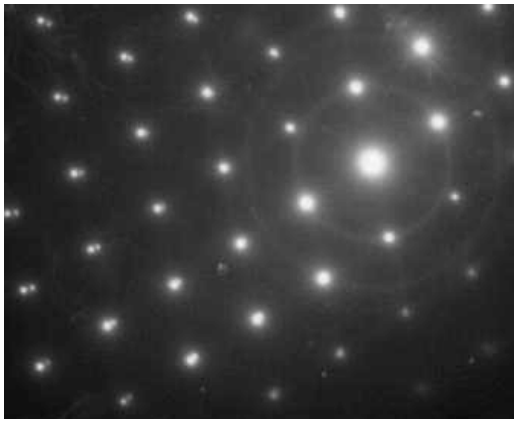

(b) Island region : B = [-1-10]

Figure 2. Selected Area Diffraction pattern for matrix and island regions.

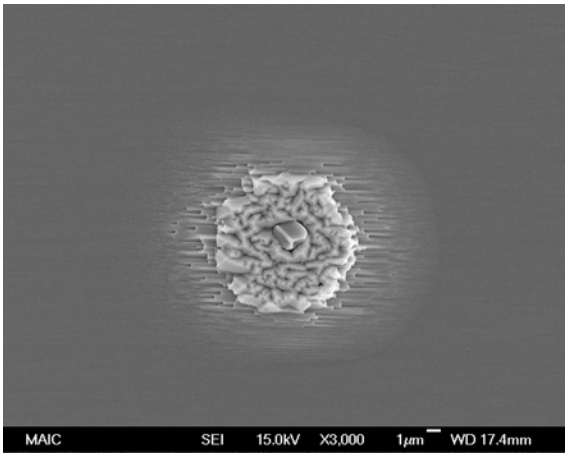

Fig. 3.3-a. Morphology of CIS-A X3,000

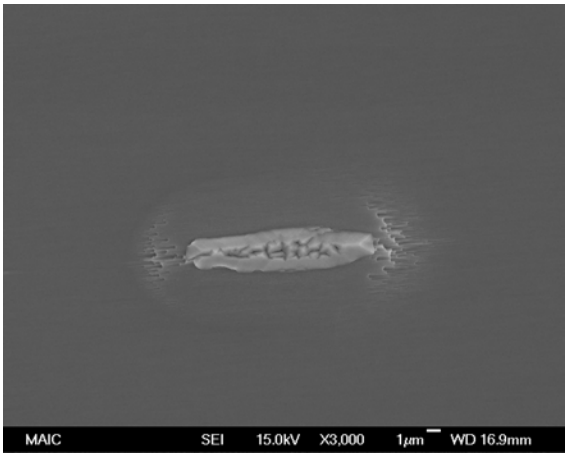

Fig. 3.3-b. Morphology of CIS-B X 3,000

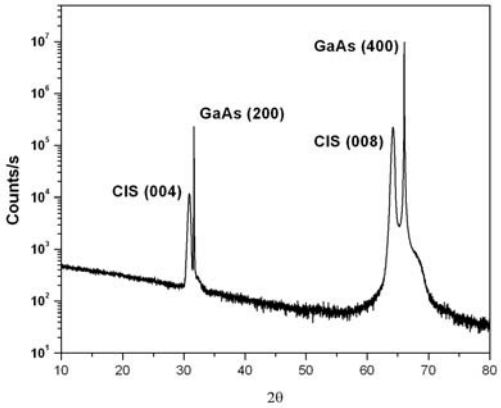

Fig. 3.4-a. XRD ω–2θ scan for CIS-A

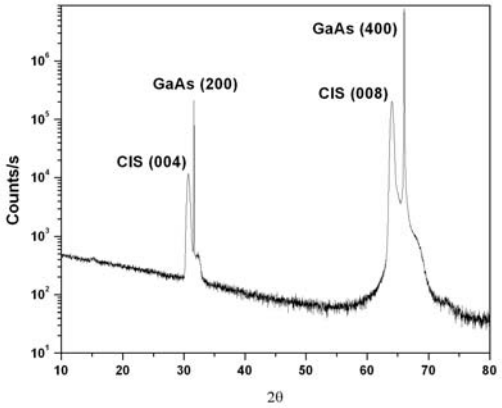

Fig. 3.4-b. XRD ω–2θ scan for CIS-B

4 Progress on Development of Alternative Buffer Layers

Participants: Sheng S. Li (Faculty Advisor) and Jiyon Song (Graduate Research Assistant)

4.1 Objectives

To develop and optimize the chemical-bath-deposited (CBD) CdS and Cd-free alternative buffer layers for CIGS-based solar cells.

4.2 Accomplishments during the current quarter

We have focused our efforts on preparing the recipes, chemicals, and deposition conditions for alternative buffer layers using (Cd,Zn)S, ZnS, and $In(OH)_xS_y$ by chemical bath deposition (CBD) for the CIGS–based solar cells. In addition, a new alternative buffer layer of $Zn_x(O,S)_y$ using modified CBD is currently in progress.

The deposition of $In(OH)_xS_y$ buffer layers is currently being investigated using 0.005M indium chloride ($InCl_3$) and 0.15M thioacetamide at around 70°C with deposition times varied. The complexing agent, acetic acid, can be added into the bath during the deposition of $In(OH)_xS_y$ to improve the film quality. In the processing, the Thioacetamide (TA) concentration and acetic acid concentration can be varied, whereas the indium chloride concentration and temperature are kept constant.

The deposition of (Cd,Zn)S buffer layers is currently under investigation using 1.2×10^{-3}M $CdCl_2$, 6.27×10^{-4}M $ZnCl_2$, 1.2×10^{-2}M thiourea, 5.27×10^{-4}M NH_3, and 1.39×10^{-3}M NH_4Cl, with the bath temperature maintained around 85°C. Different Zn compositions (x) will be used in $Cd_{1-x}Zn_xS$ by the CBD method to study the lattice-matching composition conditions and favorable conduction band alignments.

The deposition of ZnS buffer layers is currently being studied using 2.5×10^{-2}M $ZnSO_4$, 3.5×10^{-2}M thiourea, 1M NH_3, and 3M hydrazine aqueous solution with bath temperatures varied between 70 and 80°C. To compare the effect of using different recipes on absorber properties, another aqueous solution using 0.1-0.3M $ZnSO_4$, 0.4- 0.8M thiourea, and 5- 8M NH_3 will also be investigated in this study.

The aqueous solution using 0.1M $ZnSO_4$ mixed with NH_3 and 0.1M Na_2S has been used in the deposition of $Zn_x(O,S)_y$ thin films using modified chemical bath deposition (CBD) process at room temperature [1]. The glass substrate was immersed in $ZnSO_4$ solution to absorb Zn^{2+} and OH^- ions on the surface of the substrate. The substrate was rinsed in the deionized (DI) water. The glass substrate was then immersed in Na_2S solution to absorb S^{2-} ions and react with Zn^{2+} ions, and was rinsed in the DI water to remove loosely bounded particles and unreacted ions.

Such deposition steps were repeated to obtain a desired $Zn_x(O,S)_y$ film thickness. The chemical preparation and deposition conditions for $Zn_x(O,S)_y$ buffer layers are currently being investigated and the results will be discussed in next quarterly progress report.

Finally, the ZnO buffer layer, another candidate of alternative buffer layers, will be investigated to improve the light transmission in the blue wavelength region. Measurements of J-V characteristics will be performed, and the results of the ZnO deposited CIGS cells will be compared with the CIGS cells deposited with CdS buffer layers.

4.3 Activities envisioned for the next quarter

Our efforts for the CIGS-based solar cells with alternative buffer layers of (Cd,Zn)S, ZnS, and $In(OH)_xS_y$ will focus on optimizing the annealing and CBD process conditions. For buffer layers of ZnO, recipes will be developed for fabrication and characterization of the CIGS cells. Furthermore, the buffer layers of CdS and $(Cd_{1-x},Zn_x)S$ will be deposited on CIGS cells to investigate and compare the effect of different Zn compositions (x) on the performance of CIGS cells. For $Cd_{1-x}Zn_xS$, ZnS, and $In(OH)_xS_y$ thin film buffer layers deposited on glass substrates, the compositional analyses by X-ray Photoelectron Spectroscopy (XPS), analysis of crystalline phases by X-ray Diffraction (XRD), and determination of band-gap energy by spectrophotometry will be carried out.

4.4 References cited

[1] C.D. Lokhande, H.M. Pathan, M. Giersig, and H. Tributsch, "Preparation of $Zn_x(O,S)_y$ thin films using modified chemical bath deposition method," *Applied Surface Science*, Vol. 187, pp. 101-107 (2002).

5 Progress on Development of ZnO Sputtering Syatem

Participants: Oscar D. Crisalle (Faculty Advisor) and Wei Liu (Graduate Research Assistant)

5.1 Objectives

To repair and retrofit the sputtering system for the deposition of ZnO.

5.2 Accomplishments during the current quarter

5.2.1 Sputtering System Description

The system is a Perkin-Elmer 4400 series sputtering system. The system previously had three RF planar diode sources, each handling an 8 inch target in a sputter down geometry. Targets currently being used are Mo, Zn, and ZnO:Al_2O_3(98wt%:2wt%). It has been updated by adding an 8 inch diameter RF magnetron to the ZnO:Al_2O_3 target. The RF power is supplied by a Randex 2kW RF generator operating at a fixed frequency of 13.56 MHz, through an impedance matching network to the sources. The system has a switch to route the power generated by the single generator to the appropriate source or the substrate table (when sputter etching is used to clean or modify the substrate). Uniformity shields are integrated into the source, and are 1.6 cm below the target. These shields modify the geometry of the source flux to account for the higher angular velocity for increasing radial distance on the substrate platen, and thus generate a uniform film when the platen is rotated. The sources and the substrate table are cooled by chilled water. The substrate table has rotary motion capabilities, allowing deposition of uniform films on up to fourteen substrates (up to 10 cm diameter) in a single batch process. The motion system for the substrate table has been upgraded with a stepping motor, which allows more sophisticated and repeatable control of the substrate motion. Full rotation at precise speeds and accelerations, oscillations about a region below the deposition source, and accurately positioning substrates below the sources are the primary uses for the motion system. The throw, or substrate to target distance is set at 9 cm.

A stainless steel load-locked vacuum system is used to generate the vacuum required for sputter deposition. A CTI 8 cryopump and a Leybold Trivac 60cfm rotary vane pump provide the high vacuum and rough pumping, respectively. A throttle valve between the cryopump and the deposition chamber reduces the pump's effective pumping speed by up to a factor of 50 when engaged. Two mass flow controllers (MFCs) are used to regulate introduction of Ar and O_2 gas, and are used in conjunction with the throttling valve to generate a controlled gas ambient over the pressure range of 2-150 mTorr, a range typical for sputter deposition. Both MFCs have a range of 0-100 standard cubic centimeters per minute (SCCM), and control gases from ultrahigh purity gas bottles. The system operates at a typical base pressure of 1.5×10^{-7} Torr. Vacuum gauging is provided by an array of two Bayard-Alpert ionization gauges, two Convectron gauges, three thermocouple gauges, and one MKS Baratron capacitance manometer. The

Bayard-Alpert gauges are used for measurements at high vacuum conditions ($<10^{-5}$ Torr), and are therefore used to determine the base pressure of the system. The base pressure is a critical factor in controlling contamination in the growing film. The other critical gauge is the MKS Baratron gauge, which gives accurate, precise, fast, and direct measurement of the pressure for the range of 10^{-5} to 1Torr, and therefore spans the pressure range used for sputter deposition. A direct gauge refers to the fact that the gauge is sensitive directly to gas pressure, and its calibration is therefore independent of the gas being measured. This is critical for generating ambient with controlled partial pressures of a multiple gas species.

5.2.2 Activities on the Sputtering System

The there were problems with the system that have been repaired and is now in working condition. Preliminary films were deposited using the system. An Alessi four point probe was used to measure the sheet resistance and a Tencor Alpha Step 200 profiler was used to measure the thickness. Resistivity was then calculated form the results of the four point probe and profiler measurement. For a relatively thin film with ~700A thickness, the resisitvity is about $5\times10^{-3}\Omega$cm. According to the literature, increasing the film thickness will dramatically decrease the resistivity. Films reported in the literature with low resistivity typically have a thickness well over 1000A.

5.3 Activities envisioned for the next quarter

A systematic deposition study will be performed to find the optimum operating conditions for this system to deposit films with low resistivity and high transparency.